Published in final edited form as:
Acta Biomater. 2008 September ; 4(5): 1161–1171. doi:10.1016/j.actbio.2008.04.013.

Influence of hydrogel mechanical properties and mesh size on vocal fold fibroblast extracellular matrix production and phenotype

Mariah S. Hahn, **Huimin Liao**, **Dany Munoz-Pinto**, **Xin Qu**, **Yaping Hou**, and **Melissa A. Grunlan**
Texas A&M University College Station, TX, USA

Abstract

Current clinical management of vocal fold (VF) scarring produces inconsistent and often suboptimal results. Researchers are investigating a number of alternative treatments for VF lamina propria (LP) scarring, including designer implant materials for functional LP regeneration. In the present study, we investigate the effects of the initial scaffold elastic modulus and mesh size on encapsulated VF fibroblast (VFF) extracellular matrix (ECM) production toward rational scaffold design. Polyethylene glycol diacrylate (PEGDA) hydrogels were selected for this study since their material properties, including mechanical properties, mesh size, degradation rate and bioactivity, can be tightly controlled and systematically modified. Porcine VFF were encapsulated in four PEGDA hydrogels with degradation half lives of ~25 days and initial elastic compressive moduli ranging from ~30 to 100 kPa and initial mesh sizes ranging from ~9 to 27 nm. After 30 days of static culture, VFF ECM production and phenotype in each formulation was assessed biochemically and histologically. Sulfated glycosaminoglycan synthesis increased in similar degree with both increasing initial modulus and decreasing initial mesh size. In contrast, elastin production decreased with increasing initial modulus but increased with decreasing initial mesh size. Both collagen deposition and the induction of a myofibroblastic phenotype depended strongly on initial mesh size but appeared largely unaffected by variations in initial modulus. The present results indicate that scaffold mesh size warrants further investigation as a critical regulator of VFF ECM synthesis. Furthermore, this study validates a systematic and controlled approach for analyzing VFF response to scaffold properties, which should aid in rational scaffold selection/design.

Keywords

Vocal fold fibroblast; Extracellular matrix production; Rational scaffold design; Tissue engineering; Scaffold material properties; Phenotype

1. Introduction

Although no firm statistics exist, voice disorders, including scarring of the vocal fold (VF) lamina propria (LP), are estimated to affect 3–9% of the population to various degrees [1]. The VFs are paired, multi-layered structures (Fig. 1), each consisting of underlying muscle, followed by the LP and overlying epithelium [2]. When the VFs are brought together by the intrinsic laryngeal muscles, they can be set into vibratory motion by airflow from the lungs.

Ordered oscillation yields efficient cycle-to-cycle closure of the VFs and high-quality voice [3]. The human LP is generally subdivided into superficial (SLP), intermediate (ILP) and deep (DLP) layers (Fig. 1) [4,5]. At normal pitch and loudness, the SLP is believed to "slide" over the ILP, undergoing the high frequency and strain excursions required for cyclic VF closure [4,5]. When the pliability and physical volume of the VF SLP are reduced by scarring, voice changes ranging from hoarseness to complete voice loss result, depending on the severity of scar [3,6–8].

VF scar has proven difficult to treat with current surgical techniques and standard augmentation substances (e.g. collagen and fat) [3,6,9]. As such, researchers are actively exploring alternative treatment routes, including the development of designer implants for functional LP regeneration [10–15]. Although it is understood that scaffold properties, such as bioactivity [16], mesh size [17], mechanical properties [18–20] and degradation rate [21] critically impact cell behavior, it has proven difficult to directly attribute alterations in VF fibroblast (VFF) response to specific changes in scaffold parameters. This situation has hampered rational selection/design of implant materials for LP regeneration. The aim of the present study is validate an approach for the systematic and quantitative assessment of the influence of scaffold properties on VFF behavior. Specifically, the current work focuses on the impact of initial scaffold mesh size and mechanical properties on VFF extracellular (ECM) production and phenotype. Ultimately, these data will be applied toward the rational design of LP regeneration matrices.

Central to these studies is the selected scaffold material, poly(ethylene glycol) diacrylate (PEGDA). PEGDA hydrogels have several properties which make them appropriate for systematic exploration of cell response to specific alterations in scaffold material properties. Pure PEGDA hydrogels function as biological "blank slates", meaning that they do not significantly adsorb bioactive plasma proteins. Thus, these hydrogels do not promote cell interaction without the specific conjugation of biochemical stimuli to the scaffold [22]. This is significant since most synthetic and natural scaffolds adsorb a range of bioactive proteins from serum (in the in vitro setting) or from plasma (in the in vivo setting). These adsorbed proteins are often major determinants of cell behavior, in addition to any bioactive moiety deliberately conjugated or adsorbed to the scaffold [23,24]. In contrast, the biological "blank slate" nature of PEGDA hydrogels permits the controlled and defined investigation of bioactivity on cell behavior. In the present study, we explored the effects of initial PEGDA scaffold modulus and mesh size in the presence of constant initial levels of cell adhesion peptide, RGDS, thus removing initial scaffold bioactivity as a design variable [25].

An additional benefit of PEGDA hydrogels is the ability to tune their initial mesh size and mechanical properties over a broad range simply by varying the molecular weight (mol. wt.) and/or concentration of PEGDA [26]. Moreover, the degradation rate of PEG-based hydrogels can be systematically tailored. Pure PEGDA hydrogels degrade by hydrolytic cleavage of the ester bonds between the aliphatic PEG polymer backbone and the crosslinking units [27,28]. Variations in this degradation rate can be achieved by conjugating α-hydroxy acids or enzymatically cleavable peptides to the PEG macromer backbone [27,29]. Thus, PEG-based hydrogels have the property that their bioactivity, mesh size, modulus and degradation rate can each be systematically tuned [17,21,26,30], a critical property for the proposed studies.

In the present work, porcine VFF were encapsulated in four PEGDA hydrogel formulations with initial elastic compressive moduli ranging from ~30 to 100 kPa and with initial mesh sizes ranging from ~9–27 nm. To simplify the investigation of the dependence of VFF ECM synthesis and phenotype on scaffold properties, PEGDA hydrogel formulations with similar degradation rates were selected [28]. After 30 days of static culture, VFF collagen, elastin and

sulfated glycosaminoglycan (sGAG) production as well as VFF phenotype in each hydrogel formulation were analyzed using biochemical and histological techniques.

2. Material and methods

2.1. Polymer synthesis

PEGDA was prepared as previously described [31] by combining 0.1 mmol ml^{-1} dry PEG (8 or 10 kDa, Fluka), 0.4 mmol ml^{-1} acryloyl chloride and 0.2 mmol ml^{-1} triethylamine in anhydrous dichloromethane (DCM) and stirring under argon overnight. The resulting solution was washed with 2 M K_2CO_3 and separated into aqueous and DCM phases to remove HCl. The DCM phase was subsequently dried with anhydrous $MgSO_4$, and PEGDA was precipitated in diethyl ether, filtered and dried under vacuum.

2.2. Synthesis of acrylate-derivatized peptides

Cell adhesion peptide RGDS (American Peptide) was conjugated to an acrylated PEG derivative (3.4 kDa) by reaction with acryloyl-PEG-N-hydroxysuccinimide (ACRL-PEG-NHS, Nektar) at a 1:1 molar ratio for 2 h in 50 mM sodium bicarbonate buffer, pH 8.5 [31]. The product (ACRL-PEG-RGDS) was purified by dialysis, lyophilized and stored at −20 °C until use.

2.3. Hydrogel characterization

2.3.1. Hydrogel preparation—The following four hydrogel formulations were examined: (i) 10 wt.% of 10 kDa PEGDA (10% 10 kDa); (ii) 10 wt.% of 8 kDa PEGDA (10% 8 kDa); (iii) 20 wt.% of 10 kDa PEGDA (20% 10 kDa); and (iv) 30 wt.% of 10 kDa PEGDA (30% 10 kDa). Precursor solutions were prepared by dissolving PEGDA macromers and ACRL-PEG-RGDS in HEPES buffered saline (HBS; 10 mM HEPES, 150 mM NaCl, pH 7.4). The solutions were then sterilized using 0.22 μm PVDF filters, and 10 μl of a 300 mg ml^{-1} solution of photoinitiator 2,2-dimethoxy-2-phenyl-acetophenone in N-vinylpyrrolidone was added per ml precursor solution. Each solution was poured into molds composed of two glass plates separated by 1.1 mm polycarbonate spacers and then polymerized by 2 min exposure to longwave UV light (Spectroline, ~ 6 mW cm^{-2}, 365 nm) [26,32,33].

2.3.2. Hydrogel swelling—To isolate the effects of scaffold modulus and mesh size on VFF ECM production and phenotype, it was important that the cell density and bioactivity presented to the cells remain constant among formulations. Since PEGDA hydrogels swell significantly post-polymerization [34], the amount of ACRL-PEG-RGDS and cells added to each hydrogel precursor solution had to account for the change in hydrogel volume with swelling. To characterize the equilibrium swelling of each hydrogel, PEGDA hydrogels were prepared as described above. Samples (1 cm diameter) were cored from each PEGDA hydrogel immediately following polymerization and weighed. The samples were then transferred to HBS supplemented with 0.05 wt.% sodium azide (HBS-azide) and incubated at 37 °C. After 24 h, samples were blotted and weighed. Since swollen PEGDA hydrogels are primarily water, the increase in weight with swelling can be directly related to the increase in gel volume (V) with swelling, i.e. [35],

$$\left(\frac{V_{swollen}}{V_{initial}}\right)=\left(\frac{\text{swollen weight}}{\text{initial weight}}\right)$$

2.3.3. Hydrogel mesh size—PEGDA hydrogel mesh size cannot be visualized using standard techniques such as scanning electron microscopy (SEM) [36]. Thus, a variety of methods to estimate PEGDA hydrogel mesh size have been developed, including correlations linking measurable quantities, such as equilibrium hydrogel swelling, to mesh size [34,37].

Although these correlations appear to yield reasonable mesh size estimates for relatively high weight percent PEGDA hydrogels [34,37], the predictions for lower weight percent hydrogels have been called into question. Thus, in this study, hydrogel mesh size was characterized via a series of dextran diffusion experiments based on an adaptation of the methodology of Watkins et al. [38].

In brief, PEGDA hydrogels containing 2 μmol ml^{-1} ACRL-PEG-RGDS post-swelling were prepared and allowed to swell overnight at 37 °C in HBS-azide. Discs, 1 cm in diameter, were cored from each hydrogel formulation. Fluorescently labeled dextrans (10, 20, 40, 70 or 150 kDa, Sigma) were dissolved at 0.01 mg ml^{-1} in HBS-azide and added at 1 ml per hydrogel disc (3 discs per dextran mol. wt.). Dextran solutions were allowed to diffuse into the hydrogels for 24 h at 37 °C. Each gel disc was gently blotted and transferred to 1 ml fresh HBS-azide. Dextran that had penetrated into the hydrogels was then permitted to diffuse out into the surrounding solution at 37 °C. After 24 h, the fluorescence of the HBS-azide solution surrounding each disc was measured at ex/em 488/532. Dextran standard curves were used to convert each fluorescence signal to a concentration.

For the 30% 10 kDa hydrogel formulation, the dextran readings fell to background levels for dextran mol. wts. exceeding 20 kDa (data not shown). The 20 kDa dextran had a mean hydrodynamic radius of ~3.2 nm, whereas the next largest dextran investigated (40 kDa) had a mean hydrodynamic radius of ~4.5 nm [39]. Thus, the mesh size of the 30% 10 kDa hydrogel was taken to be ~(2 × 4.5) = 9 nm. The mesh sizes of the remaining formulations were calculated relative to that of the 30% 10 kDa hydrogel as follows. For each hydrogel formulation, the measured concentration readings for each dextran mol. wt. were divided by gel thickness and then plotted vs. dextran hydrodynamic radius [39]. The area (A) under the resulting curve served a quantitative indicator of hydrogel permissivity over the hydrodynamic radii range assayed. For a given hydrogel (*y*), the mesh size (ξ) could then be calculated according to the following equation:

$$\xi_x \sim \left(\frac{A_x}{A_{30\%\ 10\ kDa}}\right)(9\ nm)$$

2.3.4. Hydrogel mechanical properties—To assess the mechanical properties of the selected PEGDA formulations, hydrogels containing 2 μmol ml^{-1} ACRL-PEG-RGDS post-swelling were prepared and allowed to swell at 37 °C. After 48 h swelling, three samples, each 1.25 cm in diameter, were cored from each hydrogel and mechanically tested under unconstrained compression at room temperature using a DMA 800 (TA Instruments). During mechanical testing, samples were immersed in silicone oil to prevent hydrogel dehydration. Following application of a 0.01 N preload, each hydrogel was subjected to 10 μm cyclic compression (~1% cyclic strain) at frequencies of 0.01–100 Hz (100 Hz being the system maximum) The higher frequency testing conditions were selected to approach the frequencies of cyclic LP loading experienced during phonation [40]. The elastic and viscous compressive moduli of each hydrogel formulation were extracted from the resulting stress–strain data.

In assessing the impact of initial scaffold properties on VFF ECM production and phenotype, the elastic compressive modulus of each hydrogel formulation at 0.01 Hz (approximately static conditions) was utilized since static culture conditions were employed. In evaluating the initial mechanical properties of each PEGDA hydrogel relative to those of the VF LP, hydrogel elastic compressive moduli data at 40 Hz (mechanical measures above 40 Hz being neglected due to data quality limitations) were compared to literature values of LP elastic shear moduli at similar frequencies [40]. The fact that PEGDA hydrogels can be considered homogenous and isotropic was used in these comparisons [28,41]. For homogenous, isotropic materials, the elastic compressive modulus (*E*) is related to the elastic shear modulus (*G*) by the following

relationship: $G = E/(2+2\upsilon)$, where υ is the hydrogel Poisson ratio. For polymeric hydrogels, $\upsilon \sim 0.5$ and thus $G = E/3$ [28].

2.3.5. Hydrogel degradation rate—A PEGDA hydrogel is a three-dimensional (3-D) network of inter-crosslinked PEGDA macromers. The modulus and mesh size of this hydrogel is intimately related to the organization and density of these crosslinks. As PEGDA hydrogels degrade hydrolytically, the crosslinks among PEGDA chains are broken, resulting in a decrease in hydrogel modulus and a corresponding increase in hydrogel mesh size [42]. At the low cell densities used in the present study (~0.5×10^6 cells ml^{-1}), change in hydrogel modulus with time can be assumed to be dominated by the hydrolytic degradation of the hydrogel network rather than by ECM deposited by encapsulated cells. Thus, by monitoring the change in construct mechanical properties with time, the degradation rate of each hydrogel network can be assessed.

To confirm that our initial assumption that selected hydrogels had similar degradation rates, the compressive elastic modulus of each hydrogel formulation at day 30 was assessed according to the methodology described above. The resulting modulus data were compared to the corresponding measures at day 0 to determine a degradation half-life for each hydrogel formulation assuming first-order degradation kinetics [42].

2.4. Cell culture

Frozen VFF at passage 3 (provided by Robert Langer, ScD) [43] were thawed and cultured at 37 °C/5% CO_2 in DMEM supplemented with 10% FBS, 1 mg l^{-1} bFGF, 100 mU ml^{-1} penicillin, and 100 mg l^{-1} streptomycin (Hyclone). These VFF were isolated via primary explant [43] from the mid-membranous LP of 6- to 12-month-old pigs, a animal model commonly used for human VF LP [44]. The discarded animal tissue was obtained via the MIT Division of Comparative Medicine with the approval of and according to the guidelines of the MIT Animal Care Committee.

2.5. Cell encapsulation and hydrogel maintenance

VFF at passage 8–9 were harvested and resuspended in each precursor solution such that the post-swelling cell density would be ~0.5×10^6 cells ml^{-1}. A low cell density was selected so that the evolution in each hydrogel modulus with time could be attributed primarily to scaffold degradation. ACRL-PEG-RGDS was added to each precursor solution so that the concentration of RGDS in the swollen hydrogel would be 2 μmol ml^{-1}. The cell–precursor solution mixtures were photopolymerized into hydrogels as described above. The hydrogel slabs were transferred to Omnitrays (Nunc) fitted with four sterile polycarbonate bars to simultaneously prevent gel flotation and prevent gel contact with the tray bottom. Gels were immersed in DMEM supplemented with 10% FBS, 100 mU ml^{-1} penicillin and 100 mg l^{-1} streptomycin, and maintained at 37 °C/5% CO_2. Media was changed every 2 days. At day 30 of culture, a series of 1.25 cm diameter samples were collected from each hydrogel formulation for biochemical, histological and mechanical analyses. Mechanical analyses were conducted as described above.

2.6. Biochemical analyses

Samples harvested for biochemical analyses were transferred to screw-cap vials, weighed, flash-frozen in liquid nitrogen and stored at −80 °C. At the time of analysis, hydrogel samples were digested for 24 h at 37 °C in 1 ml of 0.1 M NaOH per 0.2 g hydrogel wet wt. [45]. The samples were then centrifuged (10,000 *g* for 10 min) and aliquots were taken for DNA and sGAG quantification. Any material pelleted during centrifugation was resuspended by vortexing, and additional hydrolysis was carried out by transferring the samples to a 100 °C oven for 90 min to solubilize collagen but not elastin [45]. These samples were then centrifuged

(10,000 *g* for 10 min) and the supernatant was retrieved for collagen quantification. The pellets (containing elastin) were washed with dIH_2O at least four times and stored at −80 °C until use.

2.6.1. DNA analysis—Aliquots of the hydrolyzed samples (n = 6 per formulation) were neutralized and their DNA content determined using the PicoGreen assay (Invitrogen) [45]. DNA measures were translated to cell number using a conversion factor of 6.6 pg DNA per cell [46]. Calf thymus DNA (Sigma) served as a standard.

2.6.2. Sulfated GAG analysis—sGAG production was measured using a modification of the Blyscan assay (Biocolor). In brief, 80 μl of each sample digest (n = 4 per formulation) was neutralized and mixed with 120 μl Blyscan dye reagent, and the absorbance at 525 nm immediately measured relative to chondroitin sulfate B (Sigma).

2.6.3. Collagen analysis—Levels of hydroxyproline were quantified as an indirect measure of total collagen. In brief, supernatants (n = 3–4 per formulation) collected for collagen quantitation were hydrolyzed for 18 h at 110 °C in 6 M HCl. Hydrolyzed samples were then dried (Centrivap, Labconco) followed by resuspension in dIH_2O and reaction with chloramine T and *p*-dimethylbenzaldehyde reagents [43]. Sample absorbance was read at 550 nm relative to that of L-4-hydroxyproline (Sigma) [43]. Total collagen content was estimated from measured grams of hydroxyproline by dividing by 0.13 [47].

2.6.4. Elastin analysis—Elastin levels were determined according to the procedure detailed in Long et al. [48]. Briefly, material pelleted following 100 °C NaOH exposure was further digested in 6 M HCl at 110 °C for 18 h. Samples (n = 3 per formulation) were then dried (Centrivap, Labconco) and the resulting free amino acids were dissolved in 100 μl of 0.1 M sodium citrate buffer (pH 5.0). Following the addition of an equal volume of ninhydrin reagent (Sigma), samples were boiled for 15 min and cooled, and their absorbance read at 570 nm. Hydrolyzed α-elastin (MP Biochemicals) was used as the standard.

The ninhydrin-based elastin readings were verified for a subset of samples (n = 2 per formulation) using direct ELISA [35] according to the following protocol. Undigested samples were hydrolyzed with 0.1 M NaOH for 24 h at 37 °C, neutralized and further digested with 0.25 M oxalic acid at 100 °C overnight. Oxalic acid was then removed and exchanged for PBS using Microcon YM-3 centrifugal filters (Millipore). Next, 100 μl of the resulting samples was applied to a high binding EIA 96 well plate (Nunc) for 3 h at room temperature. After blocking the plate with bovine serum albumin, adsorbed elastin fragments were detected by applying elastin antibody (clone B4, Santa Cruz Biotechnology, SCBT) followed by donkey anti-mouse HRP secondary antibody (SCBT) and 2,2′-azino-bis(3-ethylbenzthiazoline-6-sulphonic acid). Absorbance was read at 410 nm, with bovine aortic elastin (Sigma) serving as a standard.

For the DNA, sGAG, hydroxyproline and direct ELISA assays, the standards used were subjected to the same association with PEGDA, hydrolysis, and processing conditions as the samples. Resulting collagen, elastin and sGAG levels were normalized to cell number.

2.7. Histological analysis

Samples collected for histological analyses were fixed with 10% formalin for 30 min, embedded in Tissue-Tek media and cut into 35 μm sections. ECM deposition was analyzed in duplicate sections for each formulation using standard immunohistochemical technique. In brief, sections were exposed to Terminator (Biocare Medical) for 30 min followed by 1 h exposure to primary antibody for elastin (B4, Sigma), fibrillin-1 (12A.5, LabVision) or collagen type I (Rockland) diluted in HBS. After 30 min treatment with Peroxidase (Biocare Medical), bound primary antibody was detected using the AEC Histostain-SP kit (Invitrogen).

To detect GAG, sections were stained with toluidine blue solution (0.0714% toluidine blue, 0.0714% pyronin Y and 0.143% borax) for 6 min and rinsed with distilled water [43]. Stained sections were imaged using an Axiovert A200 microscope (Zeiss).

To identify VFF displaying a myofibroblast-like phenotype and cells undergoing proliferation, immunohistochemical staining for SM-α-actin (1A4, LabVision) was conducted as described above. For each stained section, the number of cells that stained positively for SM-α-actin was counted by two separate observers relative to total cells in each section. To assess cell proliferation, immunostaining for PCNA (Zymed) was carried out.

2.8. Comparative analyses

A plot was prepared to aid in evaluating the relative impact of scaffold modulus vs. mesh size on VFF production of collagen, elastin, and sGAG. Given the four formulations examined, there are six distinct pairwise scaffold property comparisons: (i) 10% 10 kDa vs. 10% 8 kDa; (ii) 10% 10 kDa vs. 20% 10 kDa; (iii) 10% 10 kDa vs. 30% 10 kDa; (iv) 10% 8 kDa vs. 20% 10 kDa; (v) 10% 8 kDa vs. 30% 10 kDa; and (vi) 20% 10 kDa vs. 30% 10 kDa.

For each of these *y–y* pairs, the following normalized parameters were calculated, where the subscripts “max” and “min” refer the maximum and minimum quantities, respectively, of the four formulations examined:

1. difference in initial mesh size between formulations *y* and *y* normalized to the total initial mesh size range explored (~9–27 nm):
$$|\Delta_{\text{mesh size}}|_{x-y} = \left|\left(\frac{\text{mesh size}_y - \text{mesh size}_x}{\text{mesh size}_{\max} - \text{mesh size}_{\min}}\right)\right|;$$
2. difference in initial modulus between formulations *y* and *y* normalized to the total initial elastic modulus range explored (~30–100 kPa):
$$|\Delta_{\text{modulus}}|_{x-y} = \left|\left(\frac{\text{modulus}_y - \text{modulus}_x}{\text{modulus}_{\max} - \text{modulus}_{\min}}\right)\right|;$$
3. difference in ECM component deposition relative to the maximum difference observed over the mesh size-modulus range probed:
$$\left(\Delta_{\text{ECM component}}\right)_{x-y} = \left(\frac{\text{ECM component}_y - \text{ECM component}_x}{\text{ECM component}_{\max} - \text{ECM component}_{\min}}\right);$$
4. $(\Delta_{\text{ECM component}})_{x-y}$ scaled by the by the corresponding normalized differences in initial modulus and initial mesh size:
$$\left(\Delta_{\text{ECM component}}\right)_{\text{scaled},\ x-y} = \frac{\left(\Delta_{\text{ECM component}}\right)_{x-y}}{|\Delta_{\text{mesh size}}|_{x-y}|\Delta_{\text{modulus}}|_{x-y}}.$$

This scaling procedure in (4) allowed the comparison of variations in ECM levels among *y–y* pairs irrespective of the magnitudes of the corresponding differences in modulus and mesh size $(\Delta_{\text{ECM component}})_{\text{scaled, x–y}}$ for each *y–y* pair was then plotted vs. the corresponding $\frac{|\Delta_{\text{mesh size}}|_{x-y}}{|\Delta_{\text{modulus}}|_{x-y}}$ for each ECM component. The resulting plot served as a quantitative indicator of the relative influence of modulus vs. mesh size on the production of each ECM component.

2.9. Statistical analyses

All data is reported as mean ± standard deviation. Comparison of sample means was performed using ANOVA and Tukey`s post-hoc test (SPSS software), $p < 0.05$.

3. Results

The aim of the present study was to analyze the effects of initial scaffold mesh size and elastic modulus on VFF ECM production and phenotype. To isolate these scaffold parameters, 4 PEGDA hydrogel formulations with similar degradation rates but differing moduli and mesh sizes were examined: (i) 10% 10 kDa; (ii) 10% 8 kDa; (iii) 20% 10 kDa; and (iv) 30% 10 kDa. Furthermore, cell adhesion peptide RGDS was conjugated into each hydrogel so that scaffold bioactivity could be considered a design constant.

3.1. Hydrogel mesh size, mechanical properties and degradation rate

To evaluate initial scaffold material properties, th average mesh size was evaluated for each hydrogel formulation at day 0. As previously mentioned, the mesh size of PEGDA hydrogels cannot be visualized using conventional SEM. Thus, hydrogel resistance to the diffusion of dextrans of various mol. wts. was used as a quantitative indicator of scaffold mesh size. The resulting mesh sizes are displayed in Fig. 2A. As expected, initial mesh size increased as the weight percent of PEGDA decreased [34,37].

To assess the initial mechanical environment experienced by encapsulated VFF and to confirm that the degradation rate of each hydrogel formulation was similar, the elastic compressive modulus of each hydrogel at ~1% cyclic strain was measured over a range of frequencies at days 0 and 30. To represent the scaffold stiffness experienced by cells under the selected culture conditions, static (0.01 Hz) mechanical property data are presented in Fig. 2B. Concordant with existing literature, hydrogel elastic compressive modulus at a given time-point increased significantly as PEGDA mol. wt. decreased and/or concentration increased (Fig. 2B) [45]. Furthermore, the elastic moduli of all hydrogel formulations decreased significantly from day 0 to day 30 (Fig. 2B).

Since the cell density in each hydrogel was low, the evolution in the elastic modulus of each hydrogel could be assumed to be dominated by the material degradation kinetics rather than by cell ECM deposition. Based on the modulus data at day 0 vs. day 30, the mean degradation half-life of all hydrogel formulations was determined to be 25.4 ± 3.3 days, assuming first-order degradation kinetics [42]. Thus, since each hydrogel formulation displayed a similar degradation rate, the rate of change in hydrogel elastic modulus (and, hence, hydrogel mesh size) [42] could be treated as a design “constant”. This allowed variations in VFF ECM deposition and phenotype with scaffold formulation to be evaluated relative to initial scaffold material properties without loss of information. VFF ECM production and phenotype will therefore be discussed referencing time-zero hydrogel mesh size and elastic modulus. To aid in this discussion, Fig. 2C shows a map of the time-zero mesh size–modulus sample space probed in the present study.

Note that the maximum initial mesh size explored was ~3 times that of the minimum and that the maximum initial elastic modulus was ~3.4 times the minimum. Thus, similar ranges of initial mesh size and of initial elastic modulus were explored in the present study, enhancing our ability to compare the relative impact of these two scaffold variables on VFF behavior. As demonstrated in Fig. 2A and B, the initial mesh size and elastic modulus of hydrogels formed from PEGDA macromers of a single mol. wt. cannot be independently modified (i.e. as the concentration of PEGDA is increased from 10% to 30% for the 10 kDa PEGDA hydrogels, the mesh size decreases and modulus increases). However, we can explore the effects of mesh size and elastic modulus in an uncoupled manner by appropriately varying both PEGDA concentration and mol. wt. For instance, the 10% 10 kDa and the 10% 8 kDa hydrogels have similar initial mesh sizes but significantly different initial elastic moduli. Similarly, the 10% 8 kDa hydrogel and the 20% 10 kDa hydrogels have mesh sizes that differ by ~55% but elastic moduli which differ by only ~19%.

To demonstrate that the initial mechanical properties of the selected hydrogels are within a stiffness range appropriate for VF LP tissue engineering [40], the time-zero elastic compressive modulus of each hydrogel at 40 Hz (nearer adult phonatory threshold) is presented in Fig. 2D.

3.2. Biochemical and histological analyses

PEGDA constructs were harvested at day 30 for biochemical and histological analyses. Cell density in each formulation at day 30 was >60% of the initial seeding density based upon DNA assessments, consistent with results from previous PEGDA tissue engineering studies [19]. Measured collagen, elastin and sGAG levels for each hydrogel formulation are given on a per cell basis in Fig. 3. sGAG production increased smoothly and by ~16-fold from the 10% 10 kDa to the 30% 10 kDa hydrogels ($p < 0.032$). A significant increase in collagen ($p < 0.001$) was observed at the transition between the 10% 8 kDa and 20% 10 kDa hydrogels, although no further significant change was observed progressing from the 20% 10 kDa to the 30% 10 kDa hydrogels. Elastin levels increased between the 10% 8 kDa and 20% 10 kDa hydrogels ($p < 0.001$) but then decreased proceeding to the 30% 10 kDa formulation ($p = 0.003$). A significant increase in the fraction of cells expressing SM-α-actin ($p = 0.019$) was observed from the 10% 8 kDa to the 20% 10 kDa hydrogels, although no further change was observed between the 20% 10 kDa and 30% 10 kDa hydrogels (Fig. 3D).

These results are reflected in Fig. 4, which displays a plot of $(\Delta_{\text{ECM component}})_{\text{scaled}}$ vs.the ratio $\frac{|\Delta_{\text{mesh size}}|}{|\Delta_{\text{modulus}}|}$ for each ECM component and each possible pairwise grouping of formulations, as described in Materials and Methods. The *y*-axis $(\frac{|\Delta_{\text{mesh size}}|}{|\Delta_{\text{modulus}}|})$ is plotted on a log-scale, with values less than 1 (left of the *y*-axis) representing pairwise comparisons for which $|\Delta_{\text{mesh size}}| < |\Delta_{\text{modulus}}|$ and values greater than 1 (right of *y*-axis) representing pairwise comparisons for which $|\Delta_{\text{mesh size}}| > |\Delta_{\text{modulus}}|$ For $|\Delta\text{mesh size}| < |_{\text{modulus}}|$, elastin deposition decreased, as indicated by the negative values of $(\Delta_{\text{ECM component}})_{\text{scaled}}$ In contrast, sGAG and collagen levels increased ($(\Delta_{\text{ECM component}})_{\text{scaled}} > 0$) for both $|\Delta_{\text{mesh size}}| < |\Delta_{\text{modulus}}|$ and $|\Delta_{\text{mesh size}}| > |\Delta_{\text{modulus}}|$, although the degree of the increase differed depending on whether $|\Delta_{\text{mesh size}}|$ was greater or less than $|\Delta_{\text{modulus}}|$.

Histological analyses of collagen, elastin and GAG supported the biochemical results (Fig. 5). To gain insight into the quality of elastic fiber formation, staining was also conducted for the elastin organizing microfibril, fibrillin-1. The relative intensity of fibrillin-1 staining among formulations corresponded closely with that of elastin staining, suggesting that the deposited elastin may be organizing into functional fibers, in contrast to elastin deposition in many tissue engineered situations [48]. Immunostaining for PCNA indicated heightened rates of VFF proliferation with increasing scaffold mesh size and/or decreasing modulus (data not shown).

4. Discussion

A range of scaffold properties are known to influence cell behavior, including bioactivity, mesh size, mechanical properties and degradation rate [17–21,49]. For controlled examination of the effects of various scaffold properties on cell behavior, we selected the scaffold material PEGDA. Like many scaffolds formed from synthetic materials, the mechanical properties, mesh size and degradation rate of PEGDA hydrogels can be tuned over a relatively broad range [26,50]. However, unlike most synthetic material scaffolds, PEGDA hydrogels do not significantly adsorb bioactive plasma proteins [22]. Thus, scaffold presentation of bioactive stimuli can be tightly controlled in addition to mesh size, modulusand degradation rate.

For the PEGDA hydrogels investigated (with degradation half lives of ~25 days), both VFF ECM deposition and phenotype demonstrated a strong dependence on initial hydrogel mesh

size and elastic modulus. sGAG synthesis increased both with increasing initial elastic modulus (e.g. 10% 10 kDa vs. 10% 8 kDa) and with decreasing initial mesh size (e.g. 10% 8 kDa vs. 20% 10 kDa). Further insight into the relative impact of initial mesh size vs. modulus on sGAG production can be gained by examining Fig. 4. When $|\Delta_{\text{mesh size}}|<|\Delta_{\text{modulus}}|$, $(\Delta_{\text{sGAG}})_{\text{scaled}} \sim 4$ and when $|\Delta_{\text{mesh size}}|>|\Delta_{\text{modulus}}|$, $(\Delta_{\text{sGAG}})_{\text{scaled}} \sim 2$. These results indicate that changes in initial mesh size and modulus have a similar impact on sGAG deposition, although modulus may have a slightly greater influence than mesh size. In contrast, elastin levels appeared to increase with decreasing initial mesh size (e.g. 10% 8 kDa vs. 20% 10 kDa) but to decrease with increasing initial elastic modulus (e.g. 10% 10 kDa vs. 10% 8 kDa). This was emphasized in Fig. 4, where $(\Delta_{\text{elastin}})_{\text{scaled}} < 0$ when $|\Delta_{\text{mesh size}}| < |\Delta_{\text{modulus}}|$ and $(\Delta_{\text{elastin}})_{\text{scaled}} > 0$ when $|\Delta_{\text{mesh size}}|>|\Delta_{\text{modulus}}|$. The fact that, when $|\Delta_{\text{mesh size}}| \ll |\Delta_{\text{modulus}}|$, $(\Delta_{\text{elastin}})_{\text{scaled}} \sim -8$ and that, when $|\Delta_{\text{mesh size}}| \gg |\Delta_{\text{modulus}}|$, $(\Delta_{\text{elastin}})_{\text{scaled}} \sim 8$ further suggests that effects of initial modulus and mesh size on elastin production are similar in absolute magnitude, although oppositely directed. Collagen expression increased significantly with decreasing initial mesh size (e.g. 10% 8 kDa vs. 20% 10 kDa), but appeared to be largely unaffected by alterations in initial scaffold modulus (e.g. 10% 10 kDa vs. 10% 8 kDa). Indeed, for $|\Delta_{\text{mesh size}}| \ll |\Delta_{\text{modulus}}|$, $(\Delta_{\text{collagen}})_{\text{scaled}} \sim 0$, whereas for $|\Delta_{\text{mesh size}}| \gg |\Delta_{\text{modulus}}|$, $(\Delta_{\text{collagen}})_{\text{scaled}} \sim 6$.

The relative expression of SM-α-actin, a marker indicative of fibroblast differentiation into a myofibroblast phenotype, demonstrated a similar trend as collagen (Fig. 3D). VFF are believed to transform into myofibroblasts in response to LP injury, and higher myofibroblast levels have been linked with increased collagen deposition [51]. Studies of lung and arterial tissue indicate that cell elastin [52] and GAG secretion [53] are also elevated with increasing myofibroblast phenotype. Furthermore, elevated VFF proliferation rates (fraction of cells expressing PCNA) were observed with increasing mesh size and decreasing modulus. Increased cell proliferation has frequently been correlated with decreased matrix synthesis. Thus, the increased induction of a myofibroblast-like phenotype and decreased proliferation rates observed with decreasing initial mesh size may contribute to the observed dependence of collagen, elastin and GAG levels on initial scaffold mesh size. Given the mesh sizes of the selected hydrogel formulations relative to the diameters of collagen (~4–25 nm), elastin (~2–10 nm) and moderately sized proteoglycans (~9 nm), the heightened potential of these molecules to diffuse out of the hydrogel network as mesh size increased may also contribute to the observed dependence of ECM deposition on mesh size.

A limitation of the present study is the range of mesh-size and mechanical properties probed. Future experiments will explore a broader range of initial moduli and mesh sizes as well as investigate the impact of degradation rate. A drawback of the current approach can be seen in examining Fig. 4. Despite the presence of adhesion peptide RGDS, encapsulated VFF took on rounded or stellate morphologies within the PEGDA hydrogels, in agreement with previous 3-D PEGDA studies. These morphologies are non-native for VFF in the midmembranous VF LP, in which fibroblasts generally take on spindle-shaped morphologies. The cell morphologies and pericellular localization of deposited ECM localization observed herein arise from the basic character of PEGDA hydrogels that have not been modified with additional hydrolytically or enzymatically degradable segments [19,21,30,45,54]. This particular characteristic of the selected PEGDA formulations is not optimal for fibroblasts. However, as indicated in the Introduction, PEGDA hydrogels were selected for the present study not because they are necessarily the optimal materials for vocal fold restoration, but for our ability to systematically tune their material properties. This characteristic of PEGDA hydrogels permits more controlled examination of the dependence of cell ECM production and phenotype on specific scaffold material properties, enhancing our ability to rationally design scaffolds to achieve desired cell responses.

Interestingly, the trends in collagen and elastin production with respect to alterations in initial scaffold modulus/mesh size appear to mimic those observed in native LP [55–57]. Specifically, the SLP is a relatively loose, low modulus, connective tissue, containing low levels of collagen and elastin relative to deeper regions of the LP [55–57]. The ILP and DLP are traditionally demarcated from the SLP by a marked increase in tissue density, stiffness, and elastin and collagen levels [55–57]. Thus, the initial 10% 10 kDa hydrogel material properties and stimulated ECM production correspond to those of the SLP, whereas the initial 20% 10 kDa and 30% 10 kDa hydrogel material properties and resultant ECM synthesis are more similar to those of the ILP and DLP. The correspondence between the dependence of ECM deposition with varying scaffold mesh size/modulus observed in the current work and the dependence of ECM composition with regional LP mesh size/modulus lends further strength to the present data. While it is perhaps natural that many LP bioimplant studies have focused on implant modulus rather than on microstructure [10–15] due to the LP's key biomechanical function, the present results suggest that implant mesh size may be as critical as its mechanical properties in modulating observed ECM levels.

Acknowledgements

We would like to acknowledge our funding sources, including the NIH/NIDCD and the Texas Engineering Experimental Station. We also thank Rongbin Han (Texas A&M University) and Leidy Marcela Gelves (University of Santander, Columbia) for assistance with immunostaining and acknowledge the NSF REU program for support of Caitlin Molloy, who aided in biochemical analyses in this work.

REFERENCES

1. Ramig LO, Verdolini K. Treatment efficacy: voice disorders. J Speech Lang Hear Res 1998:S101–S116. [PubMed: 9493749]
2. Gray SD. Cellular physiology of the vocal folds. Otolaryngologic Clinics of North America 2000;33 (4):679–697. [PubMed: 10918654]
3. Dailey SH, Ford CN. Surgical management of sulcus vocalis and vocal fold scarring. Otolaryngologic Clinics Of North America 2006;39(1):23–42. [PubMed: 16469653]
4. Hirano, M.; Kakita, Y. Cover-body theory of vocal fold vibration. In: Daniloff, R., editor. Speech Science. San Diego, CA: College-Hill Press; 1985. p. 1-46.
5. Kurita, S.; Nagata, K.; Hirano, M. San Diego, CA: College-Hill Press; 1983. A comparative study of the layer structure of the vocal fold; p. 3-21.
6. Benninger MS, Alessi D, Archer S, Bastian R, Ford C, Koufman J, Sataloff RT, Spiegel JR, Woo P. Vocal fold scarring: current concepts and management. Otolaryngology-Head and Neck Surgery 1996;115(5):474–482. [PubMed: 8903451]
7. Hansen JK, Thibeault SL. Current understanding and review of the literature: vocal fold scarring. Journal Of Voice 2006;20(1):110–120. [PubMed: 15964741]
8. Rosen CA. Vocal fold scar - evaluation and treatment. Otolaryngologic Clinics of North America 2000;33(5):1081–1086. [PubMed: 10984771]
9. Rosen CA. Phonosurgical vocal fold injection - procedures and materials. Otolaryngologic Clinics of North America 2000;33(5):1087–1096. [PubMed: 10984772]
10. Chan RW, Titze IR. Viscosities of implantable biomaterials in vocal fold augmentation surgery. Laryngoscope 1998;108(5):725–731. [PubMed: 9591554]
11. Chan RW, Titze IR. Hyaluronic acid (with fibronectin) as a bioimplant for the vocal fold mucosa. Laryngoscope 1999;109(7):1142–1149. [PubMed: 10401858]
12. Jia X, Burdick JA, Kobler J, Clifton RJ, Rosowski JJ, Zeitels SM, Langer R. Synthesis and characterization of in situ cross-linkable hyaluronic acid-based hydrogels with potential application for vocal fold regeneration. Macromolecules 2004;37:3239–3248.
13. Titze IR, Hitchcock RW, Broadhead K, Webb K, Li W, Gray SD, Tresco PA. Design and validation of a bioreactor for engineering vocal fold tissues under combined tensile and vibrational stresses. Journal of Biomechanics 2004;37:1521–1529. [PubMed: 15336927]

14. Hallen L, Johansson C, Laurent C. Cross-linked hyaluronan (hylan B gel): a new injectable remedy for treatment of vocal fold insufficiency – an animal study. Acta Oto-Laryngologica 1999;119(1): 107–111. [PubMed: 10219396]
15. Hallen L, Testad P, Sederholm E, Dahlqvist A, Laurent C. DiHA (dextranomers in hyaluronan) injections for treatment of insufficient closure of the vocal folds: early clinical experiences. Laryngoscope 2001;111(6):1063–1067. [PubMed: 11404622]
16. Bryant SJ, Arthur JA, Anseth KS. Incorporation of tissue-specific molecules alters chondrocyte metabolism and gene expression in photocrosslinked hydrogels. Acta Biomateralia 2005;1(2):243–252.
17. Bryant SJ, Chowdhury TT, Lee DA, Bader DL, Anseth KS. Crosslinking density influences chondrocyte metabolism in dynamically loaded photocrosslinked poly(ethylene glycol) hydrogels. Annals Of Biomedical Engineering 2004;32(3):407–417. [PubMed: 15095815]
18. Gray DS, Tien J, Chen CS. Repositioning of cells by mechanotaxis on surfaces with micropatterned Young's modulus. Journal Of Biomedical Materials Research Part A 2003;66A(3):605–614. [PubMed: 12918044]
19. Peyton SRR, Christopher B, Keschrumrus Vic P, Putnam Andrew J. The use of poly(ethylene glycol) hydrogels to investigate the impact of ECM chemistry and mechanics on smooth muscle cells. Biomaterials 2006;27:4881–4893. [PubMed: 16762407]
20. Stegemann JP, Helen H, Nerem RM. Mechanical, biochemical, and extracellular matrix effects on vascular smooth muscle cell phenotype. J Appl Physiol 2005;98:2321–2327. [PubMed: 15894540]
21. Bryant SJ, Anseth KS. Controlling the spatial distribution of ECM components in degradable PEG hydrogels for tissue engineering cartilage. Journal Of Biomedical Materials Research Part A 2003;64A(1):70–79. [PubMed: 12483698]
22. Gombotz WR, Wang GH, Horbett TA, Hoffman AS. Protein adsorption to poly(ethylene oxide) surfaces. Journal of Biomedical Materials Research 1991;25(12):1547–1562. [PubMed: 1839026]
23. Kim BS, Nikolovski J, Bonadio J, Smiley E, Mooney DJ. Engineered smooth muscle tissues: regulating cell phenotype with the scaffold. Experimental Cell Research 1999;251(2):318–328. [PubMed: 10471317]
24. Chastain SR, Kundu AK, Dhar S, Calvert JW, Putnam AJ. Adhesion of mesenchymal stem cells to polymer scaffolds occurs via distinct ECM ligands and controls their osteogenic differentiation. J Biomed Mater Res 2006;78A:73–85.
25. Hahn M, Miller J, West J. Three dimensional biochemical and biomechanical patterning of hydrogels for guiding cell behavior. Advanced Materials 2006;18(20):2679–2684.
26. Bryant SJ, Anseth KS. Hydrogel properties influence ECM production by chondrocytes photoencapsulated in poly(ethylene glycol) hydrogels. Journal Of Biomedical Materials Research 2002;59(1):63–72. [PubMed: 11745538]
27. Sawhney A, Pathak C, Hubbell J. Bioerodible hydrogels based on photopolymerized poly(ethylene glycol)-copoly(alpha-hydroxy acid) diacrylate macromers. Macromolecules 1993;26:581–587.
28. Elbert D, Hubbell JA. Conjugate addition reactions combined with free-radical cross-linking for the design of materials for tissue engineering. Biomacromolecules 2001;2:430–441. [PubMed: 11749203]
29. West J, Hubbell J. Polymeric biomaterials with degradation sites for proteases involved in cell migration. Macromolecules 1999;32:241–244.
30. Bryant SJ, Durand KL, Anseth KS. Manipulations in hydrogel chemistry control photoencapsulated chondrocyte behavior and their extracellular matrix production. Journal Of Biomedical Materials Research Part A 2003;67A(4):1430–1436. [PubMed: 14624532]
31. Hahn M, Taite L, Moon J, Rowland M, Ruffino K, West J. Photolithographic patterning of polyethylene glycol hydrogels. Biomaterials 2006;27(12):2519–2524. [PubMed: 16375965]
32. Bryant SJ, Nuttelman CR, Anseth KS. Cytocompatibility of UV and visible light photoinitiating systems on cultured NIH/3T3 fibroblasts in vitro. Journal Of Biomaterials Science-Polymer Edition 2000;11(5):439–457. [PubMed: 10896041]
33. Williams C, Malik A, Kim T, Manson P, Elisseeff J. Variable cytocompatibility of six cell lines with photoinitiators used for polymerizing hydrogels and cell encapsulation. Biomaterials 2005;26(11): 1211–1218. [PubMed: 15475050]

34. Canal T, Peppas NA. Correlation between mesh size and equilibrium degree of swelling of polymeric networks. J Biomed Mater Res 1989;23:1183–1193. [PubMed: 2808463]
35. Luo Y, Kobler JB, Zeitels SM, Langer R. Effects of growth factors on extracellular matrix production by vocal fold fibroblasts in 3-dimensional culture. Tissue Engineering 2006;12
36. Ford MC, Bertram JP, Hynes SR, Michaud M, Li Q, Young M, Segal SS, Madri JA, Lavik EB. A macroporous hydrogel for the coculture of neural progenitor and endothelial cells to form functional vascular networks in vivo. Proceedings of the National Academy of Sciences of the United States of America 2006;103(8):2512–2517. [PubMed: 16473951]
37. Mellott MB, Searcy K, Pishko MV. Release of protein from highly cross-linked hydrogels of poly (ethylene glycol) diacrylate fabricated by UV polymerization. Biomaterials 2001;22(9):929–941. [PubMed: 11311012]
38. Watkins AW, Anseth KS. Investigation of molecular transport and distributions in poly(ethylene glycol) hydrogels with confocal laser scanning microscopy. Macromolecules 2005;38(4):1326–1334.
39. Armstrong JK, Wenby RB, Meiselman HJ, Fisher TC. The hydrodynamic radii of macromolecules and their effect on red blood cell aggregation. Biophysical Journal 2004;87:4259–4270. [PubMed: 15361408]
40. Chan RW, Titze IR. Viscoelastic shear properties of human vocal fold mucosa: Measurement methodology and empirical results. Journal of the Acoustical Society of America 1999;106(4):2008–2021. [PubMed: 10530024]
41. Anseth KS, Bowman CN, BrannonPeppas L. Mechanical properties of hydrogels and their experimental determination. Biomaterials 1996;17(17):1647–1657. [PubMed: 8866026]
42. Anseth KS, Metters AT, Bryant SJ, Martens PJ, Elisseeff JH, Bowman CN. In situ forming degradable networks and their application in tissue engineering and drug delivery. Journal Of Controlled Release 2002;78(1–3):199–209. [PubMed: 11772461]
43. Hahn MS, Teply BA, Stevens MM, Zeitels SM, Langer R. Collagen composite hydrogels for vocal fold lamina propria restoration. Biomaterials 2006;27(7):1104–1109. [PubMed: 16154633]
44. Garrett CG, Coleman JR, Reinisch L. Comparative histology and vibration of the vocal folds: implications for experimental studies in microlaryngeal surgery. Laryngoscope 2000;110(5):814–824. [PubMed: 10807360]
45. Hahn M, McHale M, Wang E, Schmedlen R, West J. Physiologic pulsatile flow bioreactor conditioning of poly(ethylene glycol)-based tissue engineered vascular grafts. Annals of Biomedical Engineering 2007;35(2):190–200. [PubMed: 17180465]
46. Gregory TR. Nucleotypic effects without nuclei: genome size and erythrocyte size in mammals. Genome 2000;43(5):895–901. [PubMed: 11081981]
47. Miller EJ, Gay S. Collagen – an overview. Methods in Enzymology 1982;82:3–32. [PubMed: 7078440]
48. Long J, Tranquillo R. Elastic fiber production in cardiovascular tissue-equivalents. Matrix Biol 2003;22(4):339–350. [PubMed: 12935818]
49. Bryant SJ, Durand KL, Anseth KS. Degradation kinetics influence ECM production of photoencapsulated chondrocytes in PEG-based hydrogels. Abstracts Of Papers Of The American Chemical Society 2001;222:U244–U244.
50. Nguyen KT, West JL. Photopolymerizable hydrogels for tissue engineering applications. Biomaterials 2002;23(22):4307–4314. [PubMed: 12219820]
51. Catten M, Gray SD, Hammond TH, Zhou RX, Hammond E. Analysis of cellular location and concentration in vocal fold lamina propria. Otolaryngology-Head and Neck Surgery 1998;118(5):663–667. [PubMed: 9591866]
52. Rishikof DC, Lucey EC, Kuang P-P, Snider GL, Goldstein RH. Induction of the myofibroblast phenotype following elastolytic injury to mouse lung. Journal Histochemistry and Cell Biology 2006;125(5):527–534.
53. Shi Y, Niculescu R, Wang D, Ormont M, Magno M, San Antonio JD, Williams KJ, Zalewski A. Myofibroblast Involvement in glycosaminoglycan synthesis and lipid retention during coronary repair. Journal of Vascular Research 2000;37(5):399–407. [PubMed: 11025403]

54. Burdick JA, Anseth KS. Photoencapsulation of osteoblasts in injectable RGD-modified PEG hydrogels for bone tissue engineering. Biomaterials 2002;23(22):4315–4323. [PubMed: 12219821]

55. Gray SD, Titze IR, Alipour F, Hammond TH. Biomechanical and histologic observations of vocal fold fibrous proteins. Annals of Otology Rhinology and Laryngology 2000;109(1):77–85.

56. Hahn MS, Kobler JB, Starcher BC, Zeitels SM, Langer R. Quantitative and comparative studies of the vocal fold extracellular matrix – I: Elastic fibers and hyaluronic acid. Annals Of Otology Rhinology And Laryngology 2006;115(2):156–164.

57. Hahn MS, Kobler JB, Zeitels SM, Langer R. Quantitative and comparative studies of the vocal fold extracellular matrix – II: Collagen. Annals Of Otology Rhinology And Laryngology 2006;115(3): 225–232.

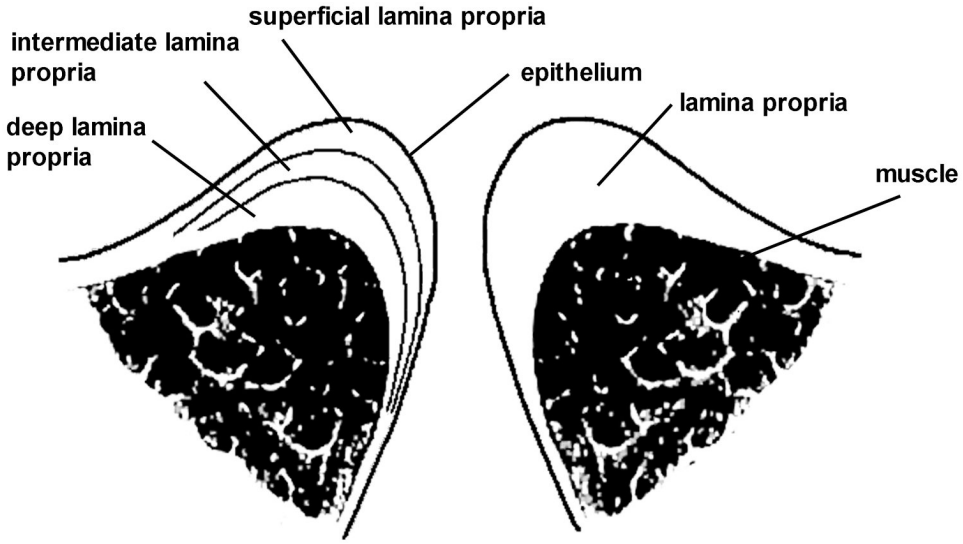

Fig. 1.
Schematic of a coronal section through the human vocal folds.

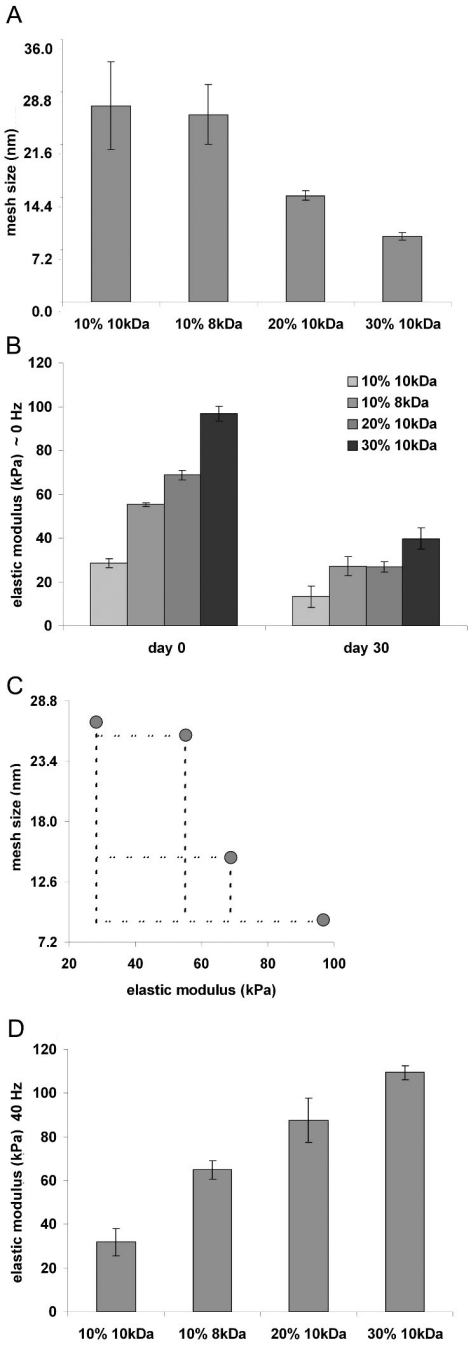

Fig. 2. Scaffold material properties

(A) Hydrogel mesh size at day 0, (B) elastic compressive modulus at approximately static (0.01 Hz) conditions at days 0 and 30, and (C) time-zero mesh size-elastic modulus sample-space. Gray dots correspond to initial mesh size-modulus combinations explored. Dashed lines are intended to highlight alterations in initial mesh size and modulus among the formulations. (D) Hydrogel elastic compressive modulus at 40 Hz at day 0.

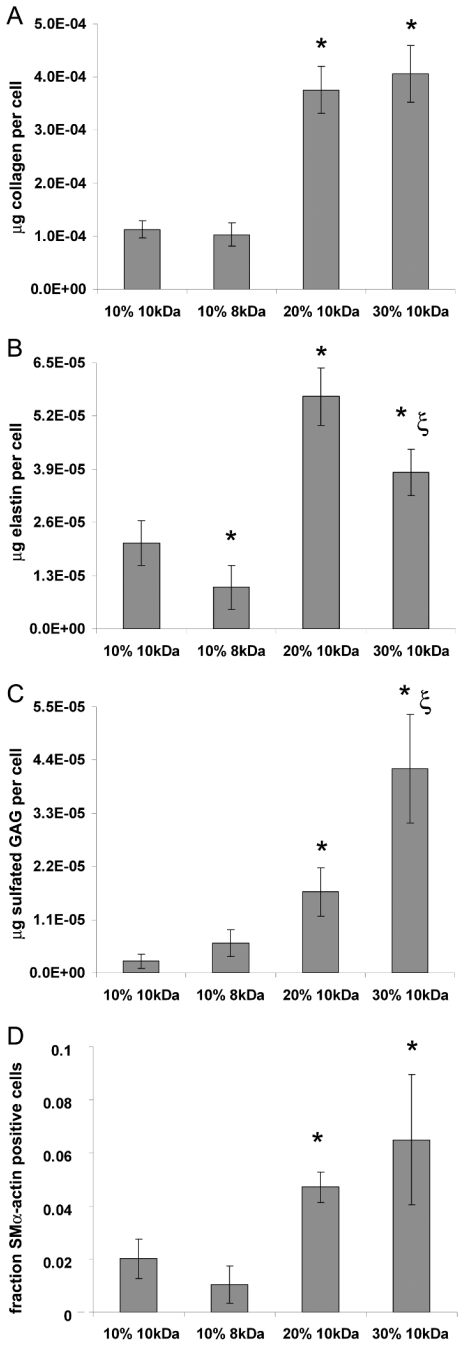

Fig. 3. Vocal fold fibroblast ECM deposition and phenotype

(A) collagen, (B) elastin, (C) sulfated glycosaminoglycan (sGAG) and (D) relative SM-α-actin expression at day 30 in each hydrogel formulation. *Significant difference with the 10% 10 kDa formulation. ξ indicates a significant difference with the 20% 10 kDa formulation.

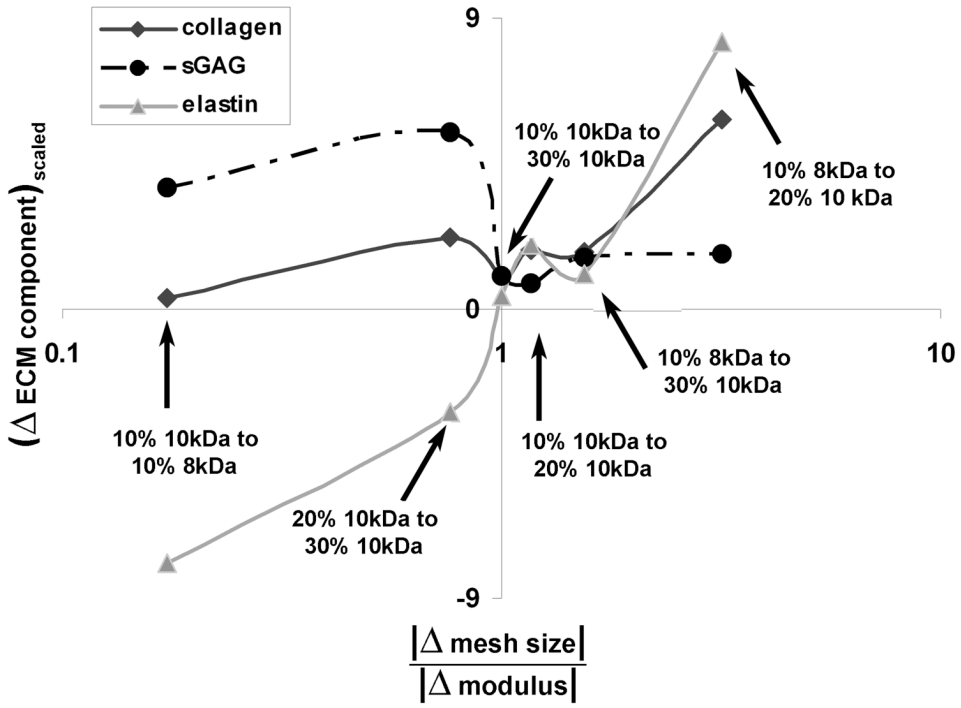

Fig. 4.

Plot of $(\Delta_{\text{ECM component}})_{\text{scaled}}$ vs. the ratio $\frac{|\Delta_{\text{mesh size}}|}{|\Delta_{\text{modulus}}|}$ for each ECM component and each pairwise grouping of formulations, as described in Materials and methods. The *y*-axis $(\frac{|\Delta_{\text{mesh size}}|}{|\Delta_{\text{modulus}}|})$ is plotted on a log-scale, with values less than 1 (left of the *y*-axis) representing pairwise comparisons for which $|\Delta_{\text{mesh size}}|<|\Delta_{\text{modulus}}|$ and values greater than 1 (right of *y*-axis) representing pairwise comparisons $|\Delta_{\text{mesh size}}|>|\Delta_{\text{modulus}}|$.

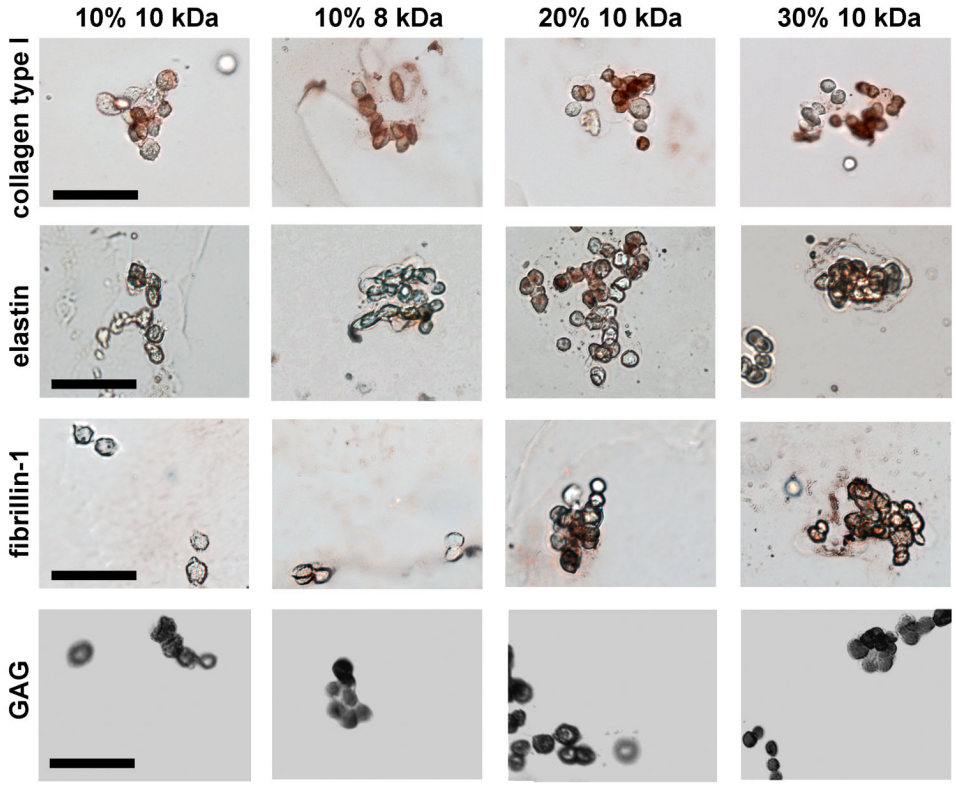

Fig. 5.
Representative images of staining for collagen type I, elastin, fibrillin-1 and GAG. GAG images are shown in grayscale to enhance contrast. Scale bars = 50 μm.